Journal of Hazardous Materials 176 (2010) 559–568

Contents lists available at ScienceDirect

Journal of Hazardous Materials

journal homepage: www.elsevier.com/locate/jhazmat

Study of the filtration performance of a plain wave fabric filter using response surface methodology

Fuping Qian*, Haigang Wang

School of Civil Engineering and Architecture, Anhui University of Technology, Hu Dong Road 59#, Ma'anshan, Anhui 243002, PR China

ARTICLE INFO

Article history:
Received 12 June 2009
Received in revised form
10 November 2009
Accepted 10 November 2009
Available online 18 November 2009

Keywords:
Plain wave fabric filter
Filtration performance
Geometry parameter
Operating condition
Response surface methodology

ABSTRACT

The gas–solid two-phase flows in the plain wave fabric filter were simulated by computational fluid dynamics (CFD) technology, and the warps and wefts of the fabric filter were made of filaments with different dimensions. The numerical solutions were carried out using commercial computational fluid dynamics (CFD) code Fluent 6.1. The filtration performances of the plain wave fabric filter with different geometry parameters and operating condition, including the horizontal distance, the vertical distance and the face velocity were calculated. The effects of geometry parameters and operating condition on filtration efficiency and pressure drop were studied using response surface methodology (RSM) by means of the statistical software (Minitab V14), and two second-order polynomial models were obtained with regard to the effect of the three factors as stated above. Moreover, the models were modified by dismissing the insignificant terms. The results show that the horizontal distance, vertical distance and the face velocity all play an important role in influencing the filtration efficiency and pressure drop of the plane wave fabric filters. The horizontal distance of 3.8 times the fiber diameter, the vertical distance of 4.0 times the fiber diameter and Reynolds number of 0.98 are found to be the optimal conditions to achieve the highest filtration efficiency at the same face velocity, while maintaining an acceptable pressure drop.

1. Introduction

In everyday life, noise and indoor air pollution are the most reported harmful effects. Beyond annoying people, indoor air pollution can have severe effects on human health because the amount of time people stay indoors occupies 80–90% of their lifetimes [1,2]. The rising awareness of environmental agencies and the general public for a clean environment together with demands of many advanced industries have urged the filtration industry to investigate on ways to improve the indoor air quality. The most common method of removing particles from a gas stream is via fibrous filters which are generally characterized by two basic parameters: filtration efficiency and pressure drop. While the current numerical studies in this area are mostly based on the media made of different materials [3–8]. Among them, Wang et al. [3] studied the permeability of multifilament woven fabrics by numerical simulation methods. Sakano et al. [4] described the influence of fiber size distribution on the filtration performance of the filter for a mass median aerodynamic diameter of fiber of 1.8 μm. However, numerical work on woven fabrics for air filtration is scarce. Indeed, the literature mostly deals with comparisons between the filtration efficiencies of different woven fabrics made of polyester/wool for submicron particles [8,9].

Concerning pressure drop modeling versus velocity, the literature presents numerous models for clean fibrous nonwoven media but information is limited for woven fabrics. An overview of available pressure drop models for woven fabrics was described in detail by Pavageau et al. [10]. Original approaches for pressure drop modeling of woven fabrics were developed by Brasquet and Le Cloirec [11], who proposed a neural network approach, and Breard et al. [12] took into account the double level of pores created by the inter-yarn and intra-yarn arrangements. In addition, there are many experimental studies dealing with the filtration efficiencies of air filters under dust loaded conditions [4,13] while few numerical simulation studies have been carried out on filtration efficiency of a woven filter. Moreover, the current studies in this area are most focus on the effect of the single factor on the filtration performance of the filter. For this purpose, a physical model of single layer plain wave fabrics is generated in this study, and the gas flow field of the plain wave fabric filter with different geometry parameters are calculated by reliable CFD simulation technology. The geometry parameters and the operating condition stated above are determined by means of response surface methodology (RSM), which enables the examination of parameters with a moderate number of experiments or CFD [14,15]. Based on RSM, the filtration efficiency of the plain wave fabrics filter is calculated by CFD approach, and

* Corresponding author. Tel.: +86 555 2311862; fax: +86 555 2311862.
E-mail address: fpingqian@gmail.com (F. Qian).

0304-3894/$ – see front matter © 2009 Elsevier B.V. All rights reserved.
doi:10.1016/j.jhazmat.2009.11.065

Table 1
Theoretical models for dimensionless pressure drop in the literature.

Researcher	Model	Classification
Happel [17]	$f(\alpha)=\frac{16\alpha}{-0.5\ \ln\alpha-0.5(1-\alpha^2/1+\alpha^2)}$	Cell theory
Kuwabrara [18]	$f(\alpha)=\frac{16\alpha}{Ku}$	Cell theory
Davies [19]	$f(\alpha)=64\alpha^{3/2}(1+56\alpha^3)$	Experimental correlation

$Ku=-0.5\ln\alpha-0.75+\alpha-0.25\alpha^2$ is the Kuwabara's hydrodynamic coefficient.

the purpose is to determine the relationship between the filtration performance and geometry parameters, which can be used for optimizing the design at a required performance level.

2. Theoretical models of the pressure drop of the filter in the literature

In the literature, the filter's pressure drop is a function of air viscosity, η, filter thickness, t, face velocity, V_{in}, fiber diameter d_f, and dimensionless pressure drop $f(\alpha)$ [16]:

$$\Delta p = f(\alpha)\frac{\eta t V_{in}}{d_f^2} \tag{1}$$

Dimensionless pressure drop is only a function of SVF (solid volume fraction), α, and has different expressions based on different theories. Different expressions of dimensionless pressure drop in the literature are presented in Table 1.

Davies's experimental correlation was obtained to calculate the pressure drop of the filter media and is proven to be accurate for a SVF range of 0.6–30%.

3. Set-up of the numerical model

3.1. Response surface methodology

Provided that the response surface is adequately fit by a second-order model, the estimated response Y for input k variables is given by Hinkelmann and Kempthorne [20]:

$$Y=\beta_0+\sum_{i=1}^{k}\beta_iX_i+\sum_{i=1}^{k}\beta_{ii}X_i^2+\sum_{i<j}\beta_{ij}X_iX_j+e(X_1,X_2,\ldots,X_k) \tag{2}$$

where X_i is the level setting of factor i, β_i, β_{ii} and β_{ij} represent regression coefficients for the linear, quadratic and interaction terms, and e is the error. There are two sources of error, *viz.* an experimental error, and a lack-of-fit error; the latter incorporates higher order terms or interactions. It was not possible to estimate the experimental error due to the deterministic character of the CFD model applied in this study; as a result, the error term only relates to the model capability.

It is assumed that the performance of plane wave fabric filter is affected by three factors, *viz.* L_1/d_f, L_2/d_f (Fig. 1) and Re ($\rho V_{in}d_f/\eta$), and the effect of the solid volume fraction (SVF) can be taken into account by the factors stated above.

A way to estimate the parameters of Eq. (2) is to study the response for all (combinations of) factors set at three different levels. This full factorial design would require $3^3=27$ different CFD calculations. However, the number of degrees of freedom (df) of the second-order model is only $2k+(1/2)k(k-1)$, which is equal to 9 for a three-factor design. A more suitable design to estimate the regression coefficients with a limited number of points of the central composite design [21] were located on a face centered hypercube, which is composed of three parts: (1) a full factorial part of 2^k vertices, (2) an axial part of $2k$ points at the origin of each factors axis, and (3) a center point. The set-up results in a central composite design of three factors demanding only 15 CFD calculations, which is a considered reduction compared to the three-level factorial design. A three-factor face central composite design is illustrated in Fig. 2.

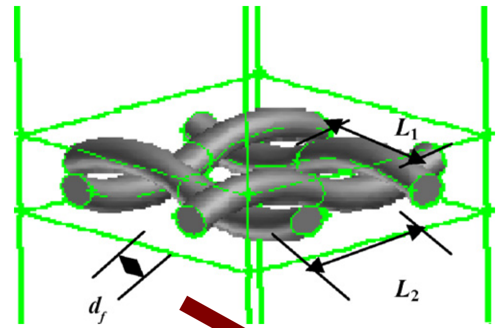

Fig. 1. Square weave yarn geometry. L_1 is the horizontal distance and L_2 is the vertical distance.

Table 2
Low and high level settings of the factors used in the response surface model.

Factor	x_i	X_{iL}	X_{iH}
L_1/d_f	x_1	3.5	4.5
L_2/d_f	x_2	3.8	4.2
Re	x_3	0.685	2.054

The regression coefficients of Eq. (2) are estimated by means of a least squares method. Since the variance of the model parameters depends on both the mean square error (MSE) and the factor magnitude, it is convenient to scale the factor level as follows [14]:

$$x_i=\frac{X_i-\overline{X_i}}{1/2(X_{iH}-X_{iL})} \tag{3}$$

where X_{iH} and X_{iL} denote the high and low level of the ith factor, respectively, and $\overline{X_i}$ is the mean level. In coded units, the high and low levels become $X_{iH}=1$ and $X_{iL}=-1$, respectively, and the mean factor level, $\overline{X_i}$, is equal to zero. Coded factor levels are used in the so-called design-model matrix, which represents all points needed in the central composite design.

3.2. Responses and factors

In Table 2, the high and low levels of the geometry parameters and operating condition are presented. The coded factor levels correspond to −1, 0, and 1 according to Eq. (3), and the factors are denoted by x_i.

The levels chosen for the Reynolds number are based on the operating for V_{in}, η and d_f. A steady state laminar incompress-

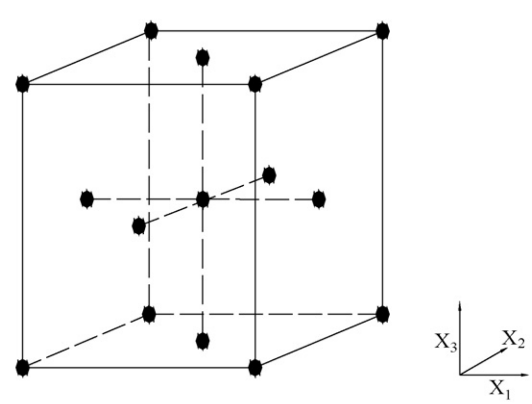

Fig. 2. A three-factor central composite design.

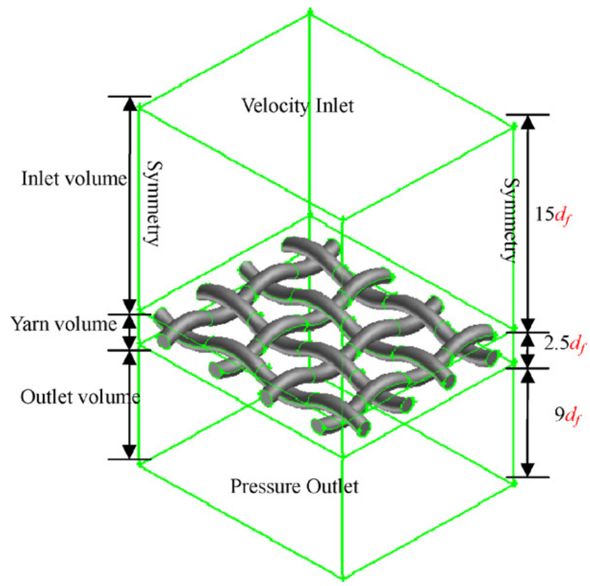

Fig. 3. Simulated geometry indicating the inlet, yarn, and outlet volumes.

ible flow is assumed to prevail inside the woven fabrics when exposed to an air flow with a velocity of 0.1 m/s [22]. This is because for the velocity and dimensions considered here, the Reynolds ($Re = \rho V_{in} d_f/\mu$) and Ma ($Ma = V_{in}/a$) numbers are too small to indicate the presence of turbulence or compressibility effects. Here ρ and μ are the air density and viscosity, respectively, while V_{in} and a are the superficial air velocity and the speed of sound.

In addition, because the restriction of geometry generating in preprocessing software, Gambit, 3.5–4.5 times the fiber diameter were chosen for the horizontal distance and vertical distance in this study. In this work, the pressure drop and filtration efficiency of the filter were assigned as the objective function, Y_i, and that the dimensionless pressure drop could be determined $K = d_f^2/f(\alpha)$ and $\Delta p = f(\alpha)(\eta t V_{in}/d_f^2)$, i.e., we chose d_f^2/K ($d_f^2/K = (\Delta p d_f^2)/(\eta t V_{in}) = f(\alpha)$) as the objective function instead of pressure drop.

3.3. CFD model

3.3.1. Meshing and boundary condition

The three-dimensional woven geometry was built within the preprocessing software, Gambit, where the CFD mesh was generated. Owing to computational time limitations, most simulations were carried out on a geometry composed of four filaments in the machine direction and cross-machine direction, as shown in Fig. 3. A brick volume was then created around the screen and the fabrics were subtracted from this volume. The brick volume was then divided into three separate volumes (Fig. 3): an inlet volume, a yarn volume, and an outlet volume. The lengths of the inlet and outlet volumes were, respectively, 15 and 9 times the fabric diameter for fear of the particles can be assumed to be not in an undisturbed flow field in an inlet volume and arising circumfluence in an outlet volume, while the length of the yarn volume was 2.5 times the diameter.

As can be seen from Fig. 3, we have used symmetry boundary for the sides of the computational box, even though there is no plane of symmetry in a fibrous structure. For the air flow on the fiber surfaces, we assumed a no-slip boundary.

The three volumes were filled with unstructured meshes. An example of the final mesh is shown in Fig. 4, the grids near the fiber was made denser in order to improve the calculation accuracy. The iteration time of every case is about 8–9 h. The CFD simulations are performed with a Pentium (R) D 2.80 GHz with 1 GB RAM-memory, and 160 GB hard disc memory. All residences are set below 10^{-5}. In order to evaluate if the results are converged, it is necessary to monitor residuals and typical variables (such as the velocity and the pressure) simultaneously. If only residuals meeting the convergence is not enough, because in which some simulated case will appear so-called pseudo-convergence [23,24]. When the residuals and variables monitored in the calculation both remain unchanged, the results will be true convergence.

3.3.2. Gas–solid two phases flow model

A steady-state laminar incompressible model has been adopted for the flow regime inside in the filter. The finite volume method [25] implemented in Fluent code is exploited to solve the airflow field. The governing equations: continuity, conservation of linear momentum, and energy written in vectorial form are as follows [3]:

$$\frac{D\rho}{Dt} + \rho\nabla \cdot V = 0 \tag{4}$$

$$\rho\frac{DV}{Dt} = -\nabla p - \eta\nabla \times (\nabla \times V) + \frac{4}{3}\eta\nabla(\nabla \cdot V) \tag{5}$$

$$\rho c_p\frac{DT}{Dt} = -\frac{Dp}{Dt} + \Phi + k\nabla^2 T \tag{6}$$

where ρ, v, p and η are the fluid density, velocity, pressure and viscosity, respectively. And in the above equations Φ, k, and c_p represent: viscous dissipation (negligible at low speeds), thermal conductivity, and the specific heat of air.

To help the solution reach the convergence, the first-order upwind scheme was used at first. Once the solution approached a stable, the second order upwind was switched to increase the accuracy.

After the particle-free flow field has been obtained, the airborne particulates, modeled by rigid spheres of uniform density $\rho = 1000\ kg/m^3$ are then introduced into the solution domain. The rational for this method is the dilution of the suspension, which leads to negligible perturbations of the continuum field by the

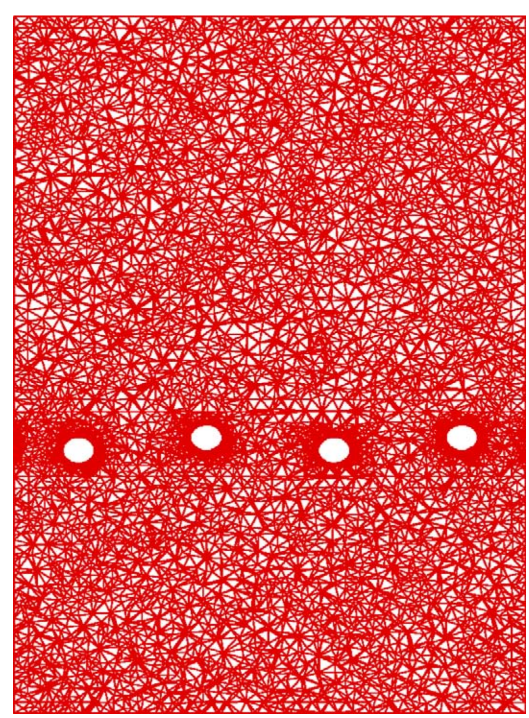

Fig. 4. Computational grids used in this study.

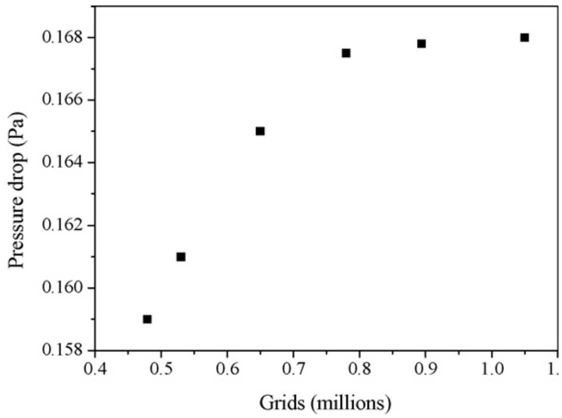

Fig. 5. Effect of the number of the grid on the pressure drop of the filter.

presence of the particulate phase [3]. Particle trajectories are then tracked via the Lagrangian method and their positions are monitored. In the Lagrangian method, the force balance on a particle is integrated to obtain the particle position in time. At the atmospheric temperature and pressure, interception plays a significant role in the filtration process, only if d_p and d_f are comparable. When $d_p/d_f \leq 1$, the interception can be always ignored [3,26]. This is the case in the present work. For particle size in this paper (0.5 μm), the diffusion and impact capture mechanisms are important in the filtration process. Therefore, the dominant forces acting on the sub-micrometer particles are drag force exerted by the flow, the Brownian force, and when $d_p \geq 1$ μm, the gravity should be included in the force balance equation:

$$\frac{dv_{i_p}}{dt} = F_d(v_i - v_{i_p}) + F_{bi} \quad (7)$$

where v_i and v_{ip} are the field and particle velocity in the x, y or z direction. F_d and F_{bi} are amplitudes of the drag ($\mathrm{Re_p} = \rho V_{in} d_p/\mu$) and Brownian force given as:

$$F_d = \frac{18\eta}{d_p^2 \rho_p C_c} \quad (8)$$

$$F_{bi} = \frac{18\mu\varsigma_i}{d_p^2 \rho_p C_c}\sqrt{\frac{2\nu}{\Delta t Sc}} \quad (9)$$

Sc is Schmidt number defined as $Sc = (3\pi d_p \mu \nu)/C_c\sigma$ ... ς_i are zero-mean, unit-variance independent Gaussian random numbers. σ is the Boltzmann constant. And the d_p is the diameter of the particle. The microparticle trajectory calculation implemented in Fluent code is originally developed by Ahmadi and his coworkers [27,28].

3.3.3. Validations of the grid dependent and the inlet particle number

Before obtaining the information about the pressure drop and filtration efficiency, the validations of the grid dependent and the inlet particle number were studied in this study, i.e., comparing the pressure drop of the filter with different grids, which is shown in Fig. 5. It can be seen that when the grids are approximately 0.9 millions, the pressure drop arrives at a stable value. Therefore, 0.9 millions were used for all geometries to ensure the accuracy of the calculations.

Filtration efficiency of the filter is determined by the number of particles it can remove from an aerosol flow [3]:

$$Y_2 = \frac{N_{in} - N_{out}}{N_{in}} \quad (10)$$

where N_{in} and N_{out} are the number of entering and exiting particles, respectively. In steady simulations, a certain number of particles are

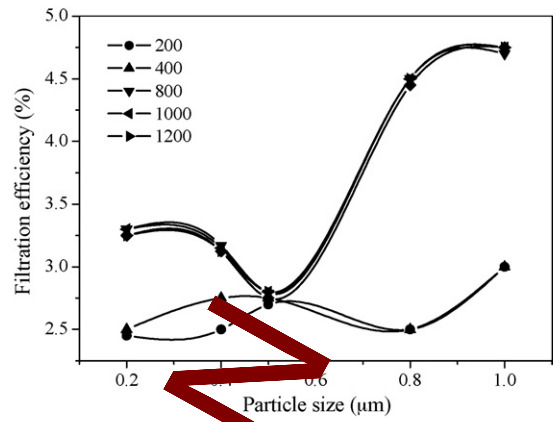

Fig. 6. Influence of the inlet particle number on the filtration efficiency of the filter.

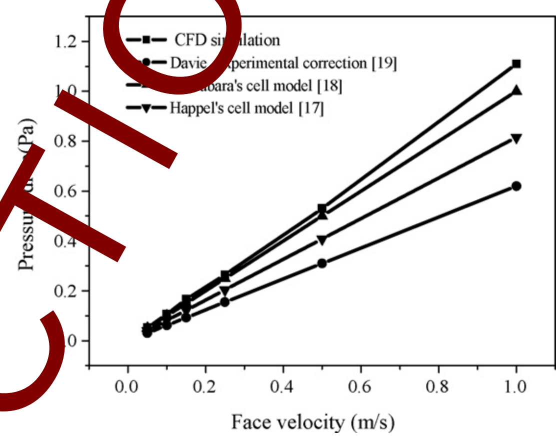

Fig. 7. Pressure drop comparison between the theoretical models and CFD simulation.

introduced into the upstream of the filter, and then their trajectories are tracked when they flow through the filter. Then N_{in} and N_{out} are compared to calculate the filtration efficiency. More particles are tracked, more accurate efficiencies are attained. In addition, the stochastic motion would generate fluctuations in the filtration efficiency from run to run. Therefore, a sensitivity test was conducted to see the influence of the particle injection on the filtration efficiency in this study. The result shows that when the inlet particle number is above 800, the filtration efficiency of the filter is almost consistent (Fig. 6). Therefore, for saving the time of outputting the data from the Fluent, 800 particles were chosen for the simulations reported in this study.

3.3.4. Validation of the numerical model

The pressure drops of the filter obtained from simulating the plane wave fabric filter and the predictions of previous theoretical models are presented in Fig. 7. It shows that there is an agreement between CFD simulations and the Kuwabrara cell model, and the error is 6.92%. Therefore, to some extent, in point of this fact, the numerical model presented in this paper can be used to predict the filtration performance of the fibrous filter.

4. Results and discussion

4.1. Analysis of variance for the whole model

The results of the CFD predictions on the pressure drop (d_f^2/K, Y_1) and filtration efficiency (Y_2, %) are summarized in Table 3 for all geometries studied.

Table 3
Central composite designs of the pressure drop (d_f^2/K), Y_1 and filtration efficiency, Y_2 (%).

No.	X_1 $\left(\frac{L_1}{d_f}\right)$	X_2 $\left(\frac{L_2}{d_f}\right)$	X_3 (Re)	Y_1 $\left(\frac{d_f^2}{K}\right)$	Y_2 (%)
1	3.5	4.0	1.3692	5.873287	3.5
2	4.5	3.8	0.6846	4.375956	3.125
3	3.5	4.2	0.6846	5.28581	3.125
4	4.0	4.0	2.0538	4.971499	4.25
5	3.5	3.8	0.6846	5.930032	3.125
6	4.0	4.0	1.3692	4.801609	3.375
7	4.5	4.0	1.3692	4.193552	3
8	4.5	3.8	2.0538	4.646623	3.875
9	4.0	4.0	0.6846	4.682687	3.000
10	4.0	4.0	1.3692	4.801609	3.375
11	4.0	4.0	1.3692	4.801609	3.375
12	4.0	4.0	1.3692	4.801609	3.375
13	4.0	4.2	1.3692	4.531265	3.25
14	3.5	3.8	2.0538	6.268023	3.875
15	3.5	4.2	2.0538	5.591804	3.5
16	4.5	4.2	2.0538	3.748951	3.125
17	4.5	4.2	0.6846	3.492448	2
18	4.0	4.0	1.3692	4.801609	3.375
19	4.0	4.0	1.3692	4.801609	3.375
20	4.0	3.8	1.3692	5.118465	3.125

Table 4
Analysis of variance for d_f^2/K.

Source	*df*	Seq *SS*	Adj *SS*	Adj *MS*	*F*-ratio	*P*-value
Regression	9	8.90752	8.90752	0.98972	376.8	0.000
Linear	3	8.78432	8.78432	2.92811	1118.26	0.000
Square	3	0.09469	0.09469	0.03156	12.02	0.001
Interaction	3	0.02851	0.02851	0.0095	3.62	0.053
Residual error	10	0.02627	0.02627	0.00263		
Lack-of-fit	5	0.02627	0.02627	0.00525		
Total	19	8.93379				

Table 5
Analysis of variance for filtration efficiency.

Source	*df*	Seq *SS*	Adj *SS*	Adj *MS*	*F*-ratio	*P*-value
Regression	9	3.20621	3.20621	0.356246	7.18	0.002
Linear	3	2.20781	2.20781	0.735938	[illegible]	0.001
Square	3	0.38317	0.38317	0.127723	[illegible]	0.112
Interaction	3	0.61523	0.61523	0.20507[illegible]	4.13	[illegible]038
Residual Error	10	0.49613	0.49613	0.049[illegible]		
Lack-of-fit	5	0.49613	0.49613	0.09[illegible]226		
Total	19	3.70234				

The results of Table 3 are used to estimate the second-order models for each response. The fitted responses are shown in Eqs. (11) and (12):

$$Y_1 = 5.2357 - 4.8376X_1 + 7.844[illegible]X_2 + [illegible].7535X_3 + 0.6877X_1^2 - 0.9159X_2^2 - 0.0734X_3^2 [illegible] 0.57[illegible]9X_1X_2 - 0.0427X_1X_3 - 0.0421X_2X_3 \quad (11)$$

$$Y_2 = -99.5136 + 16.7761X_1 + 36.2415X_2 - 1.4673X_3 - 1.0455X_1^2 - 3.4091X_2^2 + 0.6425X_3^2 - 2.3437X_1X_2 + 0.4108X_1X_3 - 0.3424X_2X_3 \quad (12)$$

The analysis of variance results for the two responses are given in Tables 4 and 5. The extremely small probability value (mostly far smaller than 0.050 for most regression terms) indicates that the calculation data are fitted well by the quadratic model, which is much higher than the 95% confidence level. The statistical analysis indicates that the proposed quadratic model for pressure drop was adequate (P [illegible] 0.0001) with satisfactory determination coefficients ($R^2 = 0.997$) (Table 6). No significant lack-of-fit of the model was found, showing that the model was sufficiently accurate for predicting the response within the range of the three factors as stated above. And yet a second-order regression model fitted filtration efficiency with accuracy ($P \le 0.002$). The determination coefficient (R^2) was 0.866 (Table 8) and the lack-of-fit was not significant, showing that the model is adequate to predict the filtration efficiency.

Table 6
Estimated regression coefficients for d_f^2/K.

Term	Coefficient	Standard error coefficient	*t*-Ratio	*P*-value
Constant	4.82557	0.01762	273.866	0.000
L_1/d	−0.84914	0.01621	−52.394	0.000
L_2/d	−0.36888	0.01621	−22.761	0.000
Re	0.14600	0.01621	9.008	0.000
$(L_1/d) \times (L_1/d)$	0.17192	0.03091	5.563	0.000
$(L_2/d) \times (L_2/d)$	−0.03664	0.03091	−1.185	0.263
Re × Re	−0.03441	0.03091	−1.113	0.292
$(L_1/d) \times (L_2/d)$	−0.05759	0.01812	−3.178	0.010
$(L_1/d) \times$ Re	−0.01460	0.01812	−0.806	0.439
$(L_2/d) \times$ Re	−0.00577	0.01812	−0.318	0.757

$S = 0.05125$; $R^2 = 99.7\%$ R^2(adj) = [illegible]%.

A determination coefficient, R^2 of 0.979 and 0.866 also suggest a good fit, which implies that the model explains 97.9% and 86.6% of the variability in the objection function, Y_i. A comparison of Y_i CFD calculated with Y_i predicted using the model is shown in Figs. 8 and 9. It shows that the model fits the CFD calculated data well in most ranges.

4.2. Effect examinations of the geometry parameters and operating condition on pressure drop

The effect examinations of coded and uncoded factors are tabulated in Tables 6 and 7. The probability value (P-value) decreases with an increasing absolute t-ratio, or the coefficient to standard error ratio. A small probability value suggests that the influence of the factor is significant. When the probability value for a factor is greater than 0.05, it means that the influential degree of the factor is lower than the 95% confidence level. For some factors, the standard error is probably even bigger than the coefficient, resulting in a probability value approaching unity, which means the factor is very uninfluential. It shows that the probability values for those terms

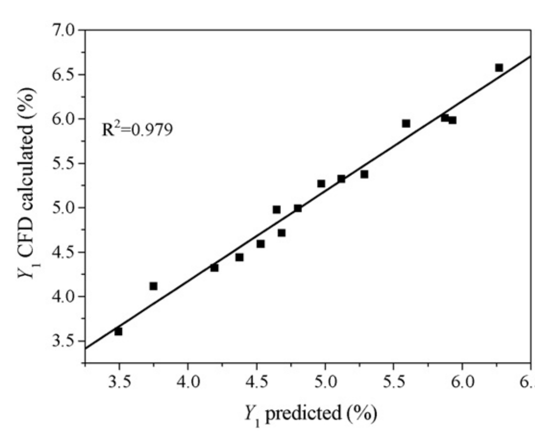

Fig. 8. A comparison of Y_1 CFD calculated with Y_1 predicted by Eq. (11).

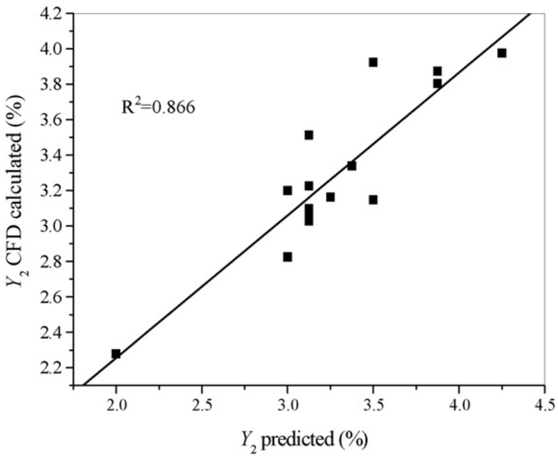

Fig. 9. A comparison of Y_2 CFD calculated with Y_2 predicted by Eq. (12).

such as constant, three linear effects (X_1, X_2 and X_3), one quadratic effect (X_1^2) and one interaction effect (X_1X_2) are lower than 0.05. This suggests that these factors have significant influences on the objective function, Y_1.

Figs. 10–12 show the relationship among L_1/d_f, L_2/d_f, and d_f^2/K with different face velocities (when Re are equal to 0.6846, 1.369 and 2.054, the corresponding face velocities are 0.05 m/s, 0.1 m/s and 0.15 m/s, respectively).

From the figures, we can see that, compared with the effect of the horizontal distance, the effect of the vertical distance on the pressure drop seems more pronounced. And yet the pressure drop decreases with the vertical distance and the horizontal distance increasing. In addition, the effect of the vertical distance and the horizontal distance on the pressure drop is changed with the different face velocity, i.e., the face velocity is 0.15 m/s, the effect of the vertical distance and the horizontal distance is stronger than the face velocity with 0.05 m/s and 0.1 m/s. Furthermore, Figs. 9–11 also show that the higher the face velocity, the greater the pressure drop, in agreement with the conclusion shown in Fig. 5.

Table 7
Estimated regression coefficients for d_f^2/K using data in uncoded units.

Term	Coefficient	Term	Coefficient
Constant	5.2357	$(L_2/d)\times(L_2/d)$	−0.9159
L_1/d	−4.8376	Re × Re	−0.0734
L_2/d	7.8443	$(L_1/d)\times(L_2/d)$	−0.5759
Re	0.7535	$(L_1/d)\times$ Re	−0.0427
$(L_1/d)\times(L_1/d)$	0.6877	$(L_2/d)\times$ Re	−0.0421

4.3. Effect examinations of the geometry parameters and operating conditions on filtration efficiency

The effect examinations of coded and uncoded factors are tabulated in Tables 8 and 9, which show that the probability values for those terms such as constant, three linear effects (X_1, X_2 and X_3), two quadratic effects (X_1^2, X_3^2) and one interaction effects (X_1X_2) are lower than 0.05. This suggests that these factors have significant influences on the objective function, Y_2.

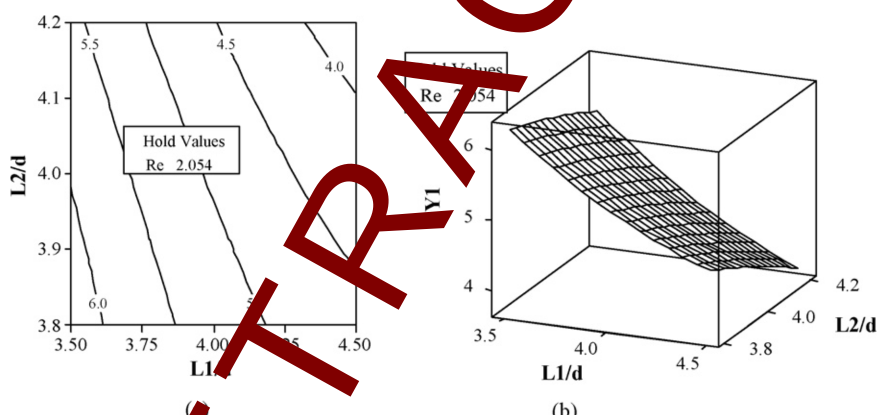

Fig. 10. (a) The X_2 vs. X_1 contour plot and (b) the corresponding surface plot, under the condition of X_3 = 2.054.

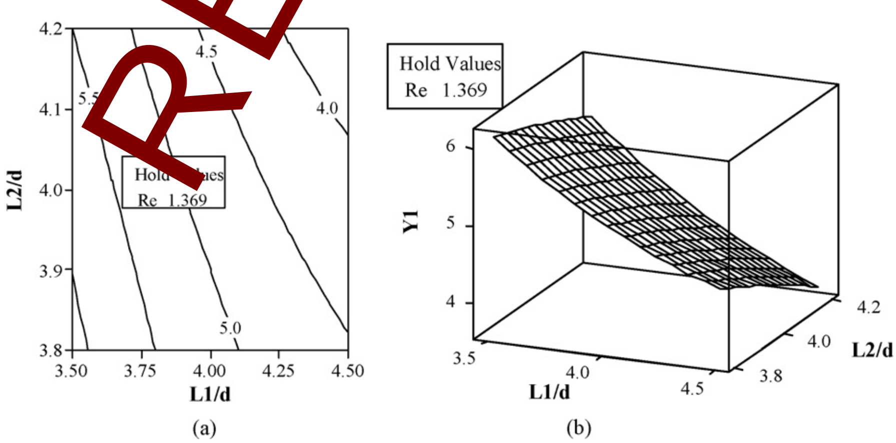

Fig. 11. (a) The X_2 vs. X_1 contour plot and (b) the corresponding surface plot, under the condition of X_3 = 1.369.

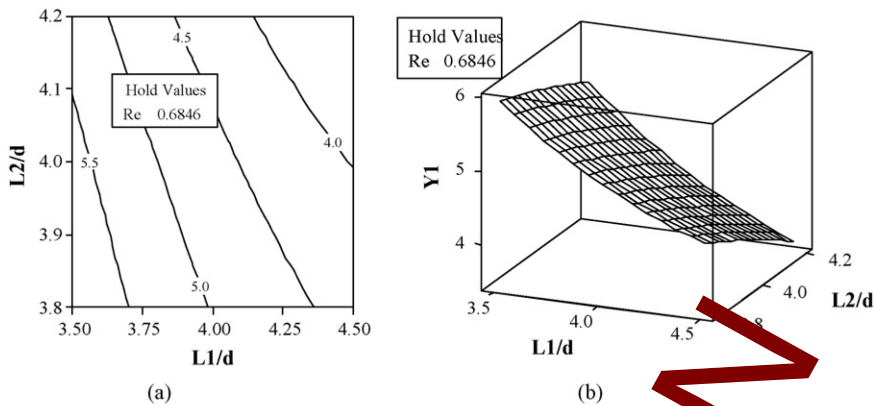

Fig. 12. (a) The X_2 vs. X_1 contour plot and (b) the corresponding surface plot, under the condition of $X_3 = 0.6846$.

Table 8
Estimated regression coefficients for filtration efficiency.

Term	Coefficient	Standard error coefficient	*t*-Ratio	*P*-value
Constant	3.35455	0.07657	43.809	0.000
L_1/d	−0.20000	0.07044	−2.839	0.018
L_2/d	−0.17500	0.07044	−2.485	0.032
Re	0.38750	0.07044	5.501	0.000
$(L_1/d)\times(L_1/d)$	−0.26136	0.13432	−1.946	0.080
$(L_2/d)\times(L_2/d)$	−0.16236	0.13432	−1.015	0.334
Re × Re	0.30114	0.13432	2.242	0.049
$(L_1/d)\times(L_2/d)$	−0.23438	0.07875	−2.976	0.014
$(L_1/d)\times$ Re	0.14063	0.07875	1.786	0.104
$(L_2/d)\times$ Re	−0.04687	0.07875	−0.595	0.565

$S = 0.2227$; $R^2 = 86.6\%$; R^2 (adj) = 74.5%.

Table 9
Estimated regression coefficients for filtration efficiency using data in uncoded units.

Term	Coefficient	Term	Coefficient
Constant	−99.5136	$(L_2/d)\times(L_2/d)$	−3.4091
L_1/d	16.7761	Re × Re	[illegible]
L_2/d	36.2415	$(L_1/d)\times(L_2/d)$	[illegible]
Re	−1.4673	$(L_1/d)\times$ Re	[illegible]
$(L_1/d)\times(L_1/d)$	−1.0455	$(L_2/d)\times$ Re	[illegible]

Figs. 13–15 show the relationship among L_1/d, L_2/d and filtration efficiency with different face velocities (when Re are equal to 0.6846, 1.369 and 2.054, the corresponding face velocities are 0.05 m/s, 0.1 m/s and 0.15 m/s, respectively).

From the figures, we can see that, the effect of the horizontal distance on the filtration efficiency seems more obvious at the low face velocity; while for the high face velocity comparing the effect of the vertical distance, while the effect of the vertical distance on filtration efficiency become significant when the face velocity is high. In addition, the effect of the vertical distance and the horizontal distance on the filtration efficiency is also changed with the different face velocity, i.e., the face velocity is 0.15 m/s, the effect of the vertical distance and the horizontal distance is stronger than the face velocity with 0.05 m/s and 0.1 m/s. Furthermore, Figs. 13–15 also show that the filtration efficiency increases with increasing the face velocity, i.e., filtration efficiency increases with the face velocity increasing for larger particle (0.5 μm), this can be interpreted that the inertia plays a greater significant role in capturing particles. Therefore, when the face velocity is high, the chance of the particle collision with the fiber is more, which leads to a higher filtration efficiency.

4.4. Modification of the response surface model

Because some terms in the model may turn out to be less significant, it would be adequate to dismiss those terms so that the model becomes more representative. In Eq. (11), 6 out 10 model terms are regarded significant. And that in Eq. (12), 7 out 10 model terms are regarded significant. Therefore, only these six terms (the constant, $X_1, X_2, X_3, X_1^2, X_1X_2$) and these seven terms (the constant, $X_1, X_2, X_3, X_1^2 X_3^2, X_1X_2$) are kept to construct a new modification model as:

$$Y_1 = 17.75 - 3.5319X_1 + 0.4593X_2 + 0.2133X_3 + 0.5172X_1^2 - 0.15759X_1X_2 \quad (13)$$

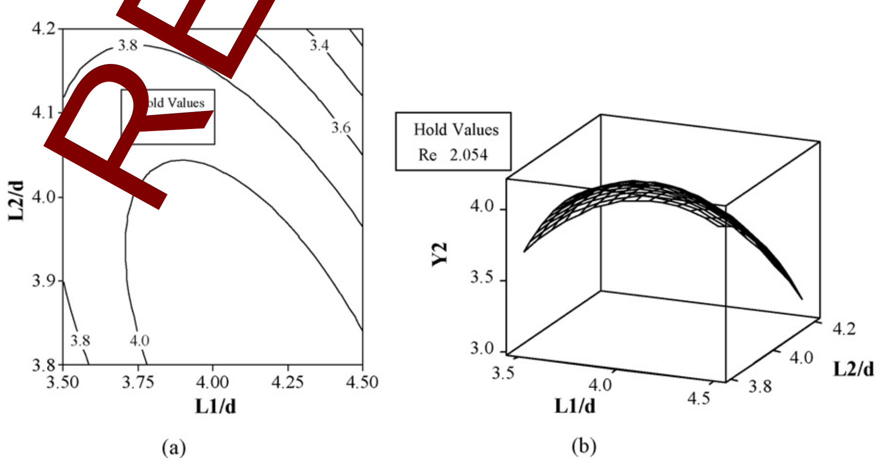

Fig. 13. (a) The X_2 vs. X_1 contour plot and (b) the corresponding surface plot, under the condition of $X_3 = 2.054$.

Table 10
Analysis of variance for d_f^2/K of the modification model.

Source	*df*	Seq *SS*	Adj *SS*	Adj *MS*	*F*-ratio	*P*-value
Regression	5	8.89444	8.89444	1.77889	632.93	0.000
Linear	3	8.78432	8.78432	2.92811	1041.82	0.000
Square	1	0.08358	0.08358	0.08358	29.74	0.000
Interaction	1	0.02653	0.02653	0.02653	9.44	0.008
Residual error	14	0.03935	0.03935	0.00281		
Total	19	8.93379				

Table 11
Analysis of variance for filtration efficiency of the modification model.

Source	*df*	Seq *SS*	Adj *SS*	Adj *MS*	*F*-ratio	*P*-value
Regression	6	2.97930	2.97930	0.496549	8.93	0.001
Linear	3	2.20781	2.20781	0.735938	13.23	0.000
Square	2	0.33203	0.33203	0.166016	2.98	0.086
Interaction	1	0.43945	0.43945	0.439453	7.90	0.015
Residual error	13	0.72305	0.72305	0.055619		
Total	19	3.70234				

$$Y_2 = -48.8375 + 18.9750X_1 + 8.5000X_2 - 0.8947X_3 - 1.2500X_1^2 + 0.5334X_3^2 - 2.3437X_1X_2 \quad (14)$$

It may be also expressed using original operating parameters as:

$$\frac{d_f^2}{K} = 17.75 - 3.5319\frac{L_1}{d} + 0.4593\frac{L_2}{d} + 0.2133\ \mathrm{Re} + 0.5172\left(\frac{L_1}{d}\right)^2 - 0.5759\frac{L_1}{d} \times \frac{L_2}{d} \quad (15)$$

$$\eta = -48.8375 + 18.975\frac{L_1}{d} + 8.5000\frac{L_2}{d} - 0.8947\ \mathrm{Re} - 1.2500\left(\frac{L_1}{d}\right)^2 + 0.5334\ (\mathrm{Re})^2 - 2.3437\frac{L_1}{d} \times \frac{L_2}{d} \quad (16)$$

To evaluate the performance of the new model, original CFD calculated data were regressed using Eqs. (13) and (14) and proceeded with the analysis of variance. The corresponding analysis of variance is tabulated in Tables 10 and 11. The extremely small probability value (far smaller than 0.050 for all regression terms) indicates that the calculation data are fitted well by the modification quadratic model.

From Table 12, both the extremely small probability value and the high R^2 value suggest a good data fit. The fact that the R^2 value approaches to the R^2 (adj) value is regarded as a result of dismissing insignificant factors in the model. Though from Table 13 the R^2 value is slightly low ($R^2 = 0.805$), it is enough satisfactory as a determination coefficient. Effect examinations of coded and uncoded factors for the two modification quadratic models were carried out and shown in Tables 12–15. They show that the significance of each factor for the objective function was greatly exalted.

vA comparison of Y_1 and Y_2 CFD calculated with Y_1 and Y_2 predicted by Eqs. (13) and (14) are shown in Figs. 16 and 17, respec-

Table 12
Estimated regression coefficients for d_f^2/K of the modification model.

Term	Coefficient	Standard error coefficient	*t*-Ratio	*P*-value
Constant	4.81136	0.01676	286.992	0.000
L_1/d	−0.84914	0.01676	−50.650	0.000
L_2/d	−0.36888	0.01676	−22.003	0.000
Re	0.14600	0.01676	8.709	0.000
$(L_1/d) \times (L_1/d)$	0.12929	0.02371	5.453	0.000
$(L_1/d) \times (L_2/d)$	−0.05759	0.01874	−3.073	0.008

$S = 0.05301$; $R^2 = 99.6\%$; R^2 (adj) = 99.4%.

Table 13
Estimated regression coefficients for filtration efficiency of the modification model.

Term	Coefficient	Standard error coefficient	*t*-Ratio	*P*-value
Constant	3.337	0.07910	42.192	0.000
L_1/d	−0.2000	0.07458	−2.682	0.019
L_2/d	−0.1750	0.07458	−2.347	0.035
Re	0.3875	0.07458	5.196	0.000
$(L_1/d) \times (L_1/d)$	−0.3125	0.13184	−2.370	0.034
Re × Re	0.2500	0.13184	1.896	0.080
$(L_1/d) \times (L_2/d)$	−0.2344	0.08388	−2.811	0.015

$S = 0.2358$; $R^2 = 80.5\%$; R^2 (adj) = 71.5%.

Table 14
Estimated regression coefficients for d_f^2/K the modification model using data in uncoded units.

Term	Coefficient	Term	Coefficient
Constant	17.75	Re	0.2133
L_1/d	−3.5319	$(L_1/d) \times (L_1/d)$	0.5172
L_2/d	0.4593	$(L_1/d) \times (L_2/d)$	−0.5759

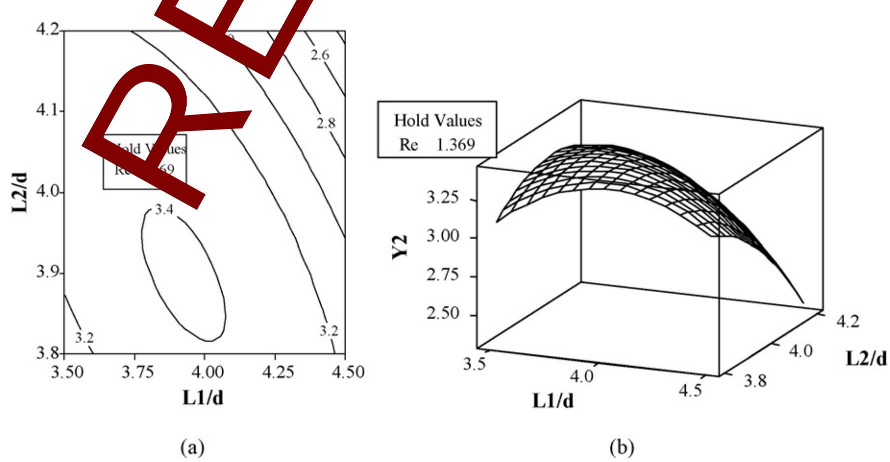

Fig. 14. (a) The X_2 vs. X_1 contour plot and (b) the corresponding surface plot, under the condition of $X_3 = 1.369$.

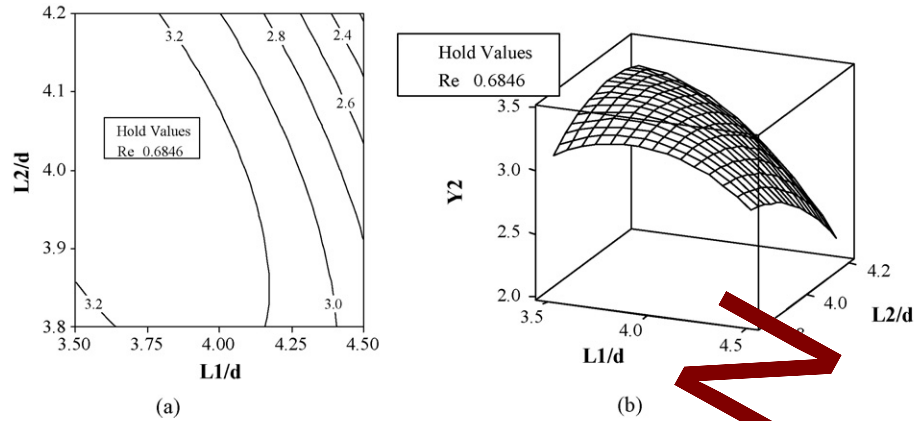

Fig. 15. (a) The X_2 vs. X_1 contour plot and (b) the corresponding surface plot, under the condition of X_3 = 0.6846.

Table 15
Estimated regression coefficients for filtration efficiency the modification model using data in uncoded units.

Term	Coefficient	Term	Coefficient
Constant	−48.8375	$(L_1/d)\times(L_1/d)$	−1.2500
L_1/d	18.975	Re × Re	0.5334
L_2/d	8.5000	$(L_1/d)\times(L_2/d)$	−2.3437
Re	−0.8947		

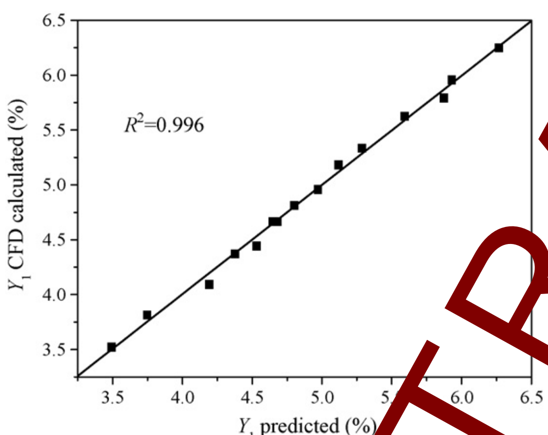

Fig. 16. A comparison of Y_1 CFD calculated with Y_1 predicted by Eq. (13).

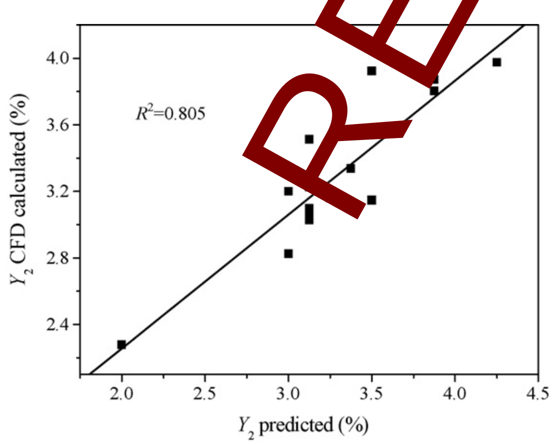

Fig. 17. A comparison of Y_2 CFD calculated with Y_2 predicted by Eq. (14).

tively. It suggested that the model is applicable in the pressure drop and filtration efficiency. This two modification RSM models for predicting pressure drop and filtration efficiency (Eq. (13), Eq. (14), respectively) with R^2 = 0.996 and R^2 = 0.805 respectively are accurate enough to predict the pressure drop and filtration efficiency of the plane wave fabric filters with different geometry parameters and operating condition.

4.5. Optimization of the process

From Figs. 10–12, we know that increasing the horizontal distance and vertical distance, the pressure drop decreased gradually, and pressure drop increased with increasing the face velocity. Therefore, there is not a maximum point within the selected range of the independent variables. However, from Fig. 14a, the filtration efficiency is increased with the increase of the horizontal distance and vertical distance at first, but after a certain value, a stationary area of filtration efficiency could be noticed, and then started to decrease. The result has shown that the response surface of the filtration efficiency has a maximum point within the experimental range of the independent variables. The precise coordinates of optimum, the levels for three independent variables were obtained by analytical procedure. The stationary point (maximum) of the fitted model was found by deriving first derivatives of the Eq. (12) [29] as follows:

$$\begin{aligned} &16.7761 - 2.081X_1 - 2.3437X_2 + 0.4108X_3 = 0 \\ &36.2415 - 6.8182X_2 - 2.3437X_1 - 0.3424X_3 = 0 \\ &-1.4673 + 1.285X_3 + 0.4108X_1 - 0.3424X_2 = 0 \end{aligned} \tag{17}$$

The system of linear Eq. (17) was solved with the help of using a numerical technique with the software Mathematics (v5.2) and the accurate optimal values of the variables were obtained: X_1 = 3.794, X_2 = 3.962 and X_3 = 0.985, which are the uncoded values of the independent factors for the maximum value of the response (filtration efficiency). The optimal values and the responses (Y_1, Y_2) are pre-

Table 16
Optimal values of the process parameter and the responses.

Independent variables	Optimal value	$Y_1\left(\frac{d_f^2}{K}\right)$	Y_2 (%)
The dimensionless horizontal distance (L_1/d)	3.8	4.670	3.289
The dimensionless vertical distance (L_2/d)	4.00		
Re	0.985		

Table 17
Comparison between the calculation values of Eqs. (11) and (12) with the value at the optimal conditions at the same face velocity (Re = 0.985).

No.	$X_1\left(\frac{L_1}{d_f}\right)$	$X_2\left(\frac{L_2}{d_f}\right)$	X_3 (Re)	$Y_1\left(\frac{d_f^2}{K}\right)$	Y_2 (%)
1	3.5	4.0	0.985	5.275	3.231
2	4.5	3.8	0.985	3.885	2.920
3	3.5	4.2	0.985	4.890	3.181
4	4.0	4.0	0.985	4.195	3.214
5	3.5	3.8	0.985	5.578	3.010
6	4.0	4.0	0.985	4.195	3.214
7	4.5	4.0	0.985	3.459	2.673
8	4.5	3.8	0.985	3.885	2.920
9	4.0	4.0	0.985	4.195	3.214
10	4.0	4.0	0.985	4.195	3.214
11	4.0	4.0	0.985	4.195	3.214
12	4.0	4.0	0.985	4.195	3.214
13	4.0	4.2	0.985	3.758	2.929
14	3.5	3.8	0.985	5.578	3.010
15	3.5	4.2	0.985	4.890	3.181
16	4.5	4.2	0.985	2.960	2.154
17	4.5	4.2	0.985	2.960	2.154
18	4.0	4.0	0.985	4.195	3.214
19	4.0	4.0	0.985	4.195	3.214
20	4.0	3.8	0.985	4.560	3.226
21	**3.8**	**4.0**	**0.985**	**4.670**	**3.289**

sented in Table 16. It could be seen that the optimal values of the responses Y_1 and Y_2 are 4.67% and 3.29%, respectively.

In addition, from the conclusions as stated above, we know that the filtration efficiency and pressure drop both increases with increasing the face velocity. Therefore, the values of the filtration efficiency and pressure drop at the same face velocity (Re = 0.985) are compared in Table 17. It could be seen that the response of the filtration efficiency at the optimal conditions is greater than any other values, at the same time maintaining an acceptable pressure drop.

5. Conclusions

Two new prediction models of the filtration efficiency and pressure drop were obtained based on response surface methodology by means of simulating gas–solid flow of plane wave fabric filter with different geometries and operating conditions, and they can be used for optimizing the design at a given required performance level. Through ANOVA analysis, the horizontal distance, the vertical distance and the face velocity play an important role in influencing the filtration efficiency and pressure drop of the plane wave fabric filters. The two modified mathematical models were shown good fit with the predicted data, since the R^2 of 0.996 and 0.805 indicated that 99.6% and 80.5% of the variability within the range of values studied could be explained by the two models. Additionally, process optimization was carried out and the optimal values of the horizontal distance (3.794 times in fiber diameter), the vertical distance (3.962 times in fiber diameter) and the Reynolds number (0.985) were thus determined. Under such optimal values, the values of the responses Y_1 and Y_2 are 4.67% and 3.29%, respectively, and the response of the filtration efficiency at the optimal conditions is greater than any other values, while maintaining an acceptable pressure drop.

Acknowledgement

This research was financially supported by the National Natural Science Foundation of China Project No. 50708001.

References

[1] R.J. Klemm, R.M. Mason, Aerosol research and inhalation epidemiological study (ARIES): air quality and daily mortality statistical modeling-interim results, Journal of Air and Waste Management Association 50 (2000) 1433–1439.
[2] N.E. Klepeis, W.C. Nelson, W.R. Ott, J.P. Robinson, A.M. Tsang, P. Switzer, J.V. Behar, S.C. Hern, W.H. Engelmann, The national human activity pattern survey (NHAPS): a resource for assessing exposure to environmental pollutants, Journal Exposure Analysis and Environmental Epidemiology 11 (2001) 231–252.
[3] Q. Wang, B. Mazea, H. Vahedi Tafreshia, A case study of simulating submicron aerosol filtration via lightweight spun-bonded filter media, Chemical Engineering Science 61 (2006) 4871–4883.
[4] T. Sakano, Y. Otani, N. Namiki, H. Emi, Particle collection of medium performance air filters consisting of binary fibers under dust loaded conditions, Separation and Purification Technology 19 (2000) 145–152.
[5] Q. Wang, H. Vahedi Tafreshi, B. Pourdeyhimi, Simulating through-plane permeability of fibrous materials having different fiber lengths, Modeling and Simulation in Materials Science and Technology 15 (2007) 855–868.
[6] S. Zobel, B. Maze, Q. Wang, H. Vahedi Tafreshi, B. Pourdeyhimi, Simulating permeability of 3D calendered fibrous structures, Chemical Engineering Science 62 (2007) 6285–6296.
[7] S. Jaganathan, H. Vahedi Tafreshi, B. Pourdeyhimi, A realistic approach for modeling permeability of fibrous media: 3D imaging coupled with CFD simulation, Chemical Engineering Science 63 (2008) 244–252.
[8] S. Green, Z. Wang, T. Waung, A. Vakil, Simulation of the flow through woven fabrics, Computers & Fluids 37 (2008) 1148–1156.
[9] S.M. Maini, S.P. Hersh, P.A. Tucker, Barrier fabrics for protection against aerosol: a review, Textile Progress 26 (1994) 1–41.
[10] M. Pavageau, L. Le Coq, J. Mabit, C. Solliec, About the applicability of commonly used pressure-flow models to plane single-layer filters of activated carbon fabric, Chemical Engineering Science 55 (2000) 2699–2712.
[11] C. Brasquet, P. Le Cloirec, Pressure drop through textile fabrics—experimental data modelling using classical models and neural networks, Chemical Engineering Science 55 (2000) 2767–2778.
[12] J. Breard, Y. Henzel, F. Trochu, R. Gauvin, Analysis of dynamic flows through porous media. Part I. Comparison between saturated and unsaturated flows in fibrous reinforcements, Polymer Composition 24 (2003) 391–408.
[13] M. Bénesse, L. Le Coq, C. Solliec, Collection efficiency of a woven filter made of multifiber yarn: experimental characterization during loading and clean filter modeling based on a two-tier single fiber approach, Journal of Aerosol Science 37 (2006) 974–989.
[14] F. Qian, M. Zhang, Study of the natural vortex length of a cyclone with response surface methodology, Computers and Chemical Engineering 29 (2005) 2155–2162.
[15] J. Zhao, B. Jin, Z. Zhong, Study of the separation efficiency of a demister vane with response surface methodology, Journal of Hazardous Materials 147 (2007) 363–369.
[16] N. Rao, M. Faghri, Computer modeling of aerosol filtration by fibrous filters, Aerosol Science Technology 8 (1988) 133–156.
[17] J. Happel, Viscous flow relative to arrays of cylinders, AIChE Journal 5 (1959) 174–177.
[18] S. Kuwabara, The forces experienced by randomly distributed parallel circular cylinders of spheres in a viscous flow at small Reynolds number, Journal of Physical Society of Japan 14 (1959) 527–532.
[19] C.N. Davies, Air Filtration, London, 1973.
[20] K. Hinkelmann, O. Kempthorne, Introduction to experimental design, in: Design and Analysis of Experiments, John Wiley and Sons, New York, 1994.
[21] G.E.P. Box, N.R. Draper, Empirical Model Building and Response Surfaces, John Wiley and Sons, New York, 1987.
[22] Q. Wang, B. Mazea, H. Vahedi Tafreshia, A note on permeability simulation of multifilament woven fabrics, Chemical Engineering Science 61 (2006) 8085–8088.
[23] R. Denschlag, M. Lingenheil, P. Tavan, Efficiency reduction and pseudo-convergence in replica exchange sampling of peptide folding–unfolding equilibria, Chemical Physical Letters 458 (2008) 244–248.
[24] E. An, J. Zhang, H. Zhou, Convergence of numerical simulations of the combustion process in utility boiler, Journal of Tongji University (Natural Science) 33 (2005) 121–125 (in Chinese).
[25] S.V. Patankar, Numerical Heat Transfer and Fluid Flow, Hemisphere Pub., Washington, 1980.
[26] F. Qian, J. Zhang, Z. Huang, Effects of the operating s and geometry parameter on the filtration performance of the fibrous filter, Chemical Engineering Technology 32 (2009) 789–797.
[27] H. Ounis, G. Ahmadi, A comparison of Brownian and turbulent diffusion, Aerosol Science Technology 13 (1990) 47–53.
[28] A. Li, G. Ahmadi, Dispersion and deposition of spherical-particles from point sources in a turbulent chemical flow, Aerosol Science Technology 6 (1992) 209–226.
[29] D. Peričin, Lj. Radulović-Popović, Ž. Vaštag, S. Madarev-Popović, S. Trivić, Enzymatic hydrolysis of protein isolate from hull-less pumpkin oil cake: application of response surface methodology, Food Chemistry 115 (2009) 753–757.